Three-Dimensional Flow Simulations for Supersonic Mixed-Compression Inlets at Incidence

Joseph Vadyak* and Joe D. Hoffman†
Purdue University, West Lafayette, Indiana
and
Allan R. Bishop‡
NASA Lewis Research Center, Cleveland, Ohio

An analysis is presented for calculating the steady three-dimensional flowfield in supersonic mixed-compression inlets at incidence. A zonal modeling approach is employed to obtain the solution. The supersonic core flow is computed using a second-order pentahedral bicharacteristic algorithm. The bow shock wave and the reflected internal shock train are determined using a three-dimensional discrete shock-fitting procedure. The boundary-layer flow adjacent to both the centerbody and the cowl is computed using a second-order implicit finite difference method. The flow in a shock-wave/boundary-layer interaction region is computed using an integral formulation. The culmination of this research effort is the development of a production-type computer program capable of analyzing the flow in a variety of mixed-compression aircraft inlets. Numerical results and correlations with experiment are presented to illustrate application of the analysis.

Nomenclature

h = mean static enthalpy per unit mass
H = mean stagnation enthalpy per unit mass
h_1, h_2 = metric coefficients
$\hat{i}, \hat{j}, \hat{k}$ = unit vectors in the x, y, and z directions
K_1, K_2 = geodesic curvature terms
L = mixing length
$\dot{m}_{\text{bleed}}$ = bleed mass flow rate
M = Mach number
$\hat{n}_b$ = unit vector normal to a solid boundary
P = pressure
P_T = stagnation pressure
Pr = laminar Prandtl number
Pr_t = turbulent Prandtl number
R_c = cowl lip radius
$\hat{t}$ = unit vector along shock/boundary intersection
$\tilde{u}, \tilde{v}, \tilde{w}$ = mean velocity components in the $\tilde{x}$, $\tilde{y}$, and $\tilde{z}$ directions
x, y, z = Cartesian coordinates
$\tilde{x}, \tilde{y}, \tilde{z}$ = boundary-layer orthogonal curvilinear coordinates
α = angle-of-attack or turbulence model constant
γ = specific heat ratio
δ = boundary-layer thickness
δ_{TR} = intermittency factor
ϵ = turbulent eddy viscosity
ϵ_θ = turbulent eddy thermal conductivity
η = normal coordinate
μ = dynamic viscosity
ρ = density
ϕ, ψ = vector potential functions

Subscripts

e = boundary-layer edge conditions
w = wall conditions
$\tilde{x}, \tilde{y}, \tilde{z}$ = partial derivative with respect to $\tilde{x}$, $\tilde{y}$, and $\tilde{z}$
∞ = freestream conditions

Superscripts

$( )'$ = time fluctuation or partial derivative with respect to η
$(\bar{})$ = time average or space average

Introduction

THE objective of this investigation[1] was to develop a method to compute the steady three-dimensional flowfield in supersonic mixed-compression aircraft inlets at incidence. A typical axisymmetric mixed-compression inlet is shown in Fig. 1. Compression occurs both in the external flow about the forebody and in the internal flow inside the annulus. A bow shock wave emanates from the forebody tip. An internal shock wave emanates from the cowl lip and reflects a number of times between the centerbody and the cowl before terminating in the divergence downstream of the geometric throat of the annulus. The core flow is subsonic downstream of that location.

Two-dimensional or axisymmetric analyses applicable to zero incidence cases have been developed for inlets such as that of Fig. 1. Sorensen,[2] Anderson et al.,[3] and Reyhner and Hickcox[4] have developed spatial marching algorithms based on two-dimensional method of characteristics procedures. More recently, Knight[5] has computed high-speed inlet flows using a time-dependent two-dimensional Navier-Stokes algorithm which employs the explicit MacCormack finite difference operator.[6]

Presley,[7] Buggeln et al.,[8] and Vadyak and Hoffman[9] have developed spatial marching algorithms for simulating the three-dimensional flow in supersonic inlets at incidence. Presley[7] employed the explicit MacCormack finite difference operator[6] in developing a shock-capturing algorithm for

Presented as Paper 82-0061 at the AIAA 20th Aerospace Sciences Meeting, Orlando, Fla., Jan. 11-14, 1982; submitted Jan. 22, 1982; revision received Aug. 30, 1983.

*Visiting Assistant Professor of Mechanical Engineering. Presently, Scientist, Advanced Flight Sciences Department, Lockheed-Georgia Co., Marietta, Ga. Member AIAA.

†Professor of Mechanical Engineering, Thermal Sciences and Propulsion Center. Member AIAA.

‡Member of Propulsion Aerodynamics Division.

solution of the supersonic inviscid flow. Buggeln et al.[8] are developing a noniterative shock-capturing parabolized Navier-Stokes algorithm. Vadyak and Hoffman[9] have developed a second-order pentahedral bicharacteristic algorithm used in conjunction with a discrete shock-wave fitting procedure for simulating three-dimensional inviscid or weakly viscous high-speed inlet flows. An independent evaluation of the algorithms presented in Refs. 7 and 9 may be found in Ref. 10. The purpose of the present paper is to report an extension of the analysis of Vadyak and Hoffman[9] which includes computation of the boundary-layer effects within the inlet.

A zonal modeling approach is employed in which the flowfield is divided into different computational regimes, as shown in Fig. 1. The regimes consist of the supersonic core flow, the centerbody and cowl boundary layers, and the shock-wave/boundary-layer interaction regions on both the centerbody and cowl. An appropriate analysis is used for each of the different regimes.

The supersonic core flow is characterized by a hyperbolic system of governing equations. That system is solved using a second-order pentahedral bicharacteristic algorithm. The bow shock wave and the reflected internal shock-wave system are computed using a discrete shock-wave fitting procedure.

The boundary-layer flow is characterized by a parabolic system of governing equations. That system is solved using a second-order implicit finite difference scheme which can compute both positive and negative cross flows. The finite difference algorithm is used to compute all of the boundary-layer flow except for that in the shock-wave/boundary-layer interaction regions.

The shock-wave/boundary-layer interaction region flow is characterized by an elliptic system of governing equations. The flow for this region is computed using an integral analysis which yields property profiles downstream of the interaction region. The profiles are then used as starting data for the analysis of the boundary-layer flow downstream of the interaction region using the implicit finite difference algorithm.

Calculation of the Supersonic Core Flow

The method used to calculate the supersonic core flow is presented in Refs. 1 and 11 and will only be summarized herein.

The equations of motion for supersonic flow form a hyperbolic system of five nonlinear nonhomogeneous partial differential equations. Two families of characteristic surfaces exist for this system: stream surfaces and wave surfaces. Stream surfaces are composed of streamlines. Wave surfaces are tangent to a Mach conoid with the line of tangency between a given wave surface and the conoid being a bicharacteristic. The original system of equations is replaced by a system of five compatibility relations written in terms of directional derivatives along streamlines and bicharacteristics. An explicit second-order numerical integration scheme was devised based upon Butler's bicharacteristic parameterization.[12] The influence of molecular transport may be included in the solution by treating the viscous and thermal diffusion terms in the governing equations as source terms.

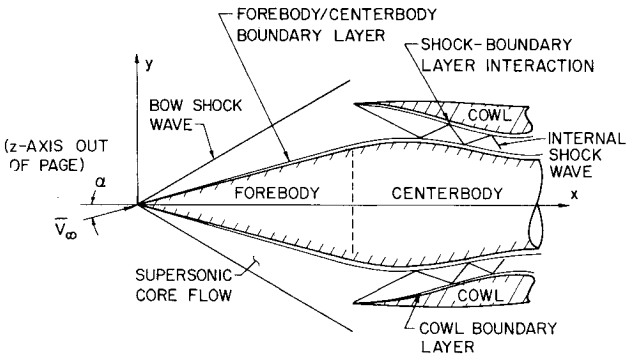

Fig. 1 Mixed-compression inlet.

The bow shock wave surrounding the forebody and the internal shock-wave system are determined by discrete shock-wave fitting. The continuous flow between shock waves is determined by the characteristic procedure, and the flow properties across the shock waves are determined by applying the Rankine-Hugoniot jump conditions.

In the supersonic flow algorithm, an inverse marching scheme is employed. The solution is obtained on space-like planes of constant x, where the x axis is the longitudinal axis of the inlet. For the internal flow, the solution is also obtained on the space curves which are defined by the intersections of the internal shock wave with the solid boundaries. Except in the vicinity of a shock-wave/solid-boundary intersection, the distance Δx between successive solution planes is determined by the Courant-Friedrichs-Lewy (CFL) stability criterion. In the vicinity of a shock-wave intersection with a solid boundary, the distance between solution planes is chosen so that the entire shock-wave/solid-boundary intersection falls between two adjacent solution planes.

Governing Equations for the Boundary-Layer Flow

The parabolic equations of motion for the boundary-layer flow have been derived in orthogonal curvilinear coordinates by Vaglio-Laurin.[13] The orthogonal coordinate system used for the boundary-layer computation is composed of the coordinates $\tilde{x}$, $\tilde{y}$, and $\tilde{z}$; where $\tilde{x}$ is coincident with the body surface and lies in a given meridional plane, $\tilde{y}$ is orthogonal to the body surface, and $\tilde{z}$ is orthogonal to both $\tilde{x}$ and $\tilde{y}$.

For steady three-dimensional flow, the boundary-layer governing equations are given by

$$(\rho h_2 \tilde{u})_{\tilde{x}} + (\rho h_1 \tilde{w})_{\tilde{z}} + (h_1 h_2 \rho \overline{\tilde{v}})_{\tilde{y}} = 0 \tag{1}$$

$$\rho\tilde{u}\tilde{u}_{\tilde{x}}/h_1 + \rho\tilde{w}\tilde{u}_{\tilde{z}}/h_2 + \rho\overline{\tilde{v}}\tilde{u}_{\tilde{y}} - \rho\tilde{u}\tilde{w}K_2 + \rho\tilde{w}^2K_1 = -P_{\tilde{x}}/h_1 + (\mu\tilde{u}_{\tilde{y}} - \rho\overline{\tilde{u}'\tilde{v}'})_{\tilde{y}} \tag{2}$$

$$\rho\tilde{u}\tilde{w}_{\tilde{x}}/h_1 + \rho\tilde{w}\tilde{w}_{\tilde{z}}/h_2 + \rho\overline{\tilde{v}}\tilde{w}_{\tilde{y}} - \rho\tilde{u}\tilde{w}K_1 + \rho\tilde{u}^2K_2 = -P_{\tilde{z}}/h_2 + (\mu\tilde{w}_{\tilde{y}} - \rho\overline{\tilde{w}'\tilde{v}'})_{\tilde{y}} \tag{3}$$

$$\rho\tilde{u}H_{\tilde{x}}/h_1 + \rho\tilde{w}H_{\tilde{z}}/h_2 + \rho\overline{\tilde{v}}H_{\tilde{y}} = \{\mu H_{\tilde{y}}/Pr + \mu(1-1/Pr)[(\tilde{u}^2+\tilde{w}^2)/2]_{\tilde{y}} - \rho\overline{\tilde{v}'\tilde{H}'}\}_{\tilde{y}} \tag{4}$$

Equations (1-4) represent the continuity, streamwise momentum, cross-flow momentum, and energy equations, respectively. Boundary conditions for the preceding equations may be written as

$$\tilde{y}=0: \quad \tilde{u}=0, \quad \tilde{w}=0, \quad \tilde{v}=\tilde{v}_w(\tilde{x},\tilde{z})$$

$$H=H_w(\tilde{x},\tilde{z}) \text{ or } H_{\tilde{y}}=H'_w(\tilde{x},\tilde{z}) \tag{5}$$

$$\tilde{y}=\delta: \quad \tilde{u}=\tilde{u}_e(\tilde{x},\tilde{z}), \tilde{w}=\tilde{w}_e(\tilde{x},\tilde{z}) \quad H=H_e(\tilde{x},\tilde{z}) \tag{6}$$

Limiting forms of the above equations are employed on a plane of flow symmetry (i.e., the leeward and windward meridians). These equations, generally referred to as the attachment line equations, are discussed in detail in Ref. 1.

Turbulent closure is achieved by using the two-layer eddy viscosity model of Cebeci et al.[14] Using this model, the Reynolds stress terms are represented as

$$-\rho\overline{\tilde{u}'\tilde{v}'}=\rho\epsilon_x\tilde{u}_{\tilde{y}} \tag{7}$$

$$-\rho\overline{\tilde{w}'\tilde{v}'}=\rho\epsilon_z\tilde{w}_{\tilde{y}} \tag{8}$$

$$-\rho\overline{H'\tilde{v}'}=\rho\epsilon_\theta H_{\tilde{y}} \tag{9}$$

Isotropic turbulence has been assumed, hence, $\epsilon_x=\epsilon_z$.

For the inner layer ($0\le\tilde{y}\le\tilde{y}_T$), the eddy viscosity ϵ_i is given by the mixing length expression

$$\epsilon_x=\epsilon_z=\epsilon_i=\delta_{TR}L^2(\tilde{u}_{\tilde{y}}^2+\tilde{w}_{\tilde{y}}^2)^{1/2} \tag{10}$$

where $\tilde{y}_T$ is the distance from the wall where $\epsilon_i=\epsilon_0$ (ϵ_0 is the eddy viscosity for the outer layer), L is the mixing length, and δ_{TR} is a streamwise intermittency factor accounting for the progressive transition from laminar to turbulent flow. The mixing length L employs the van Driest damping factor and accounts for both the streamwise pressure gradient and wall mass transfer. The intermittency factor δ_{TR} is based on the exponential function proposed by Dhawan and Narasimha.[15] It is applied in a meridional plane sense, which allows for a circumferential variation in transition onset location.

For the outer layer ($\tilde{y}_T\le\tilde{y}\le\delta$), the eddy viscosity ϵ_0 is given by the velocity defect expression

$$\epsilon_x=\epsilon_z=\epsilon_0=\Delta_{TR}\alpha\left|\int_0^\infty[(\tilde{u}_e^2+\tilde{w}_e^2)^{1/2}-(\tilde{u}^2+\tilde{w}^2)^{1/2}]\,d\tilde{y}\right| \tag{11}$$

where the constant α is taken as 0.0168. The turbulent thermal conductivity ϵ_θ is given by

$$\epsilon_\theta=(\epsilon_x^2+\epsilon_z^2)^{1/2}/Pr_t \tag{12}$$

where the turbulent Prandtl number Pr_t is taken as 0.90 and is assumed to be constant across the boundary layer.

The boundary-layer equations are solved using the transformed variables proposed by Moore.[16] A two-component vector potential is defined such that

$$\rho h_2\tilde{u}=\psi_{\tilde{y}}\quad \rho h_1\tilde{w}=\phi_{\tilde{y}}\quad h_1h_2\overline{\rho\tilde{v}}=-(\psi_{\tilde{x}}+\phi_{\tilde{z}})+h_1h_2(\rho\tilde{v})_w \tag{13}$$

The governing equations are transformed from the $(\tilde{x},\tilde{y},\tilde{z})$ space to the $(\tilde{x},\eta,\tilde{z})$ space where

$$d\eta=(\tilde{u}_e/\rho_e\mu_e\tilde{x})^{1/2}\rho\,d\tilde{y} \tag{14}$$

The functions ψ and ϕ take the forms

$$\psi=(\rho_e\mu_e\tilde{u}_e\tilde{x})^{1/2}h_2f(\tilde{x},\eta,\tilde{z})$$

$$\phi=(\rho_e\mu_e\tilde{u}_e\tilde{x})^{1/2}h_1(\tilde{w}_e/\tilde{u}_e)g(\tilde{x},\eta,\tilde{z}) \tag{15}$$

where f and g are to be determined numerically. Substituting Eqs. (13-15) into the governing equations [note that Eqs. (1) is identically satisfied] yields

$$[C(1+\epsilon_x^+)f'']'+P_2ff''+P_3gf''$$

$$+(M/h_1)[(\rho_e/\rho)-(f')^2]+P_4[(\rho_e/\rho)-(g')^2]$$

$$+P_5[g'f'-(\rho_e/\rho)]-Tf''=(\tilde{x}/h_1)(f'f'_{\tilde{x}}-f''f_{\tilde{x}})$$

$$+(\tilde{w}_e\tilde{x}/\tilde{u}_eh_2)(g'f'_{\tilde{z}}-f''g_{\tilde{z}}) \tag{16}$$

for Eq. (2), with similar expressions being obtained for Eqs. (3) and (4), where primes denote differentiation with respect to η. The parameters C, M, T, P_2, P_3, P_4, and P_5 are functions of the external flow and/or wall conditions and are presented in Ref. 1. The parameter ϵ_k^+ denotes the respective turbulent transport coefficient divided by the kinematic viscosity, and

$$f'=\tilde{u}/\tilde{u}_e,\quad g'=\tilde{w}/\tilde{w}_e,\quad \theta=H/H_e \tag{17}$$

The boundary conditions for the transformed equations are given by

$$\eta=0\text{: } f=0,\ g=0,\ f'=0,\ g'=0,\ \theta=\theta_w \text{ or } \theta'=\theta'_w \tag{18}$$

$$\eta=\eta_\delta\text{: } f'=1,\ g'=1,\ \theta=1 \tag{19}$$

A similar set of transformed equations can be derived for the attachment line equations. Those results are presented in Ref. 1.

Solution of the Boundary-Layer Equations

The transformed boundary-layer equations are solved using a second-order semi-implicit finite difference algorithm in which marching is performed in the $\tilde{x}$ direction. The numerical algorithm is based on the Keller box scheme[17] which has been applied to the computation of three-dimensional flows by Cebeci et al.[18] To compute the boundary-layer flow, three types of differencing schemes are employed. The choice of which scheme to use depends upon whether the cross-flow velocity is positive, negative, or identically zero (plane of symmetry flow). The differencing schemes for positive and negative cross flow will be briefly discussed herein.

The algorithm is based on solving a system of first-order equations. The transformed streamwise momentum, cross-flow momentum, and energy equations can be written as a first-order system by defining the following variables:

$$f'=u,\ u'=v,\ g'=w,\ w'=t,\ \theta'=\Delta \tag{20}$$

where the primes denote differentiation with respect to η. Introducing Eq. (20) into Eqs. (16) yields the first-order equation

$$bv'+(b'+P_2f+P_3g-T)v+M(\lambda-u^2)/h_1+P_4(\lambda-w^2)$$

$$+P_5(uw-\lambda)=\tilde{x}(uu_{\tilde{x}}-vf_{\tilde{x}})/h_1+\tilde{w}_e\tilde{x}(wu_{\tilde{z}}-vg_{\tilde{z}})/\tilde{u}_eh_2 \tag{21}$$

Similar expressions hold for the cross-flow momentum and energy equations.

The difference equations are solved for positive cross-flow velocities ($\tilde{w}>0$) using the computational network illustrated in Fig. 2, where k_{n-1}, h_{j-1}, and r_{i-1} denote the step sizes in the $\tilde{x}$, η, and $\tilde{z}$ directions, respectively. The finite difference equations used to approximate Eqs. (20) are obtained by using centered difference and averaging expressions taken about point 1 in Fig. 2, which is located midway between the points $(\tilde{x}_n, n_j, \tilde{z}_i)$ and $(\tilde{x}_n, n_{j-1}, \tilde{z}_i)$. The finite difference approximation to Eq. (21) is obtained by using centered difference and averaging expressions taken about point 2 in Fig. 2, which is the midpoint of the computational cell. In a similar manner, difference expressions are also obtained for the transformed cross-flow momentum and energy equations.

Taken with the boundary conditions, the preceding finite difference equations form a system of $8N$ equations for the $8N$ unknowns along the boundary layer normal (containing N points) located at $\tilde{x}=\tilde{x}_n$ and $\tilde{z}=\tilde{z}_i$, provided that the properties at stations $(\tilde{x}_n, \tilde{z}_{i-1})$, $(\tilde{x}_{n-1}, \tilde{z}_i)$, and $(\tilde{x}_{n-1}, \tilde{z}_{i-1})$ are known. The system of difference equations is solved implicitly using Newton's method with a direct matrix solution procedure. The details of the solution procedure are given in Ref. 1.

Due to numerical stability considerations, first explained by Raetz,[19] alterations to the above scheme must be made when attempting to compute boundary-layer flows with a negative cross-flow velocity component. The first-order system of transformed equations is solved for negative cross-flow cases using the computational network illustrated in Fig. 3. The computational cell is now staggered in the $\tilde{z}$ direction. The finite difference equations used to approximate Eqs. (20) are obtained by using centered difference and averaging expressions taken about point 1 in Fig. 3, which is located midway between the points $(\tilde{x}_n, n_j, \tilde{z}_i)$ and $(\tilde{x}_n, n_{j-1}, \tilde{z}_i)$. The finite difference approximation to Eq. (21) is obtained by using centered difference and averaging expressions taken about points 2, 3, and 4 in Fig. 3, which are the midpoints of the three faces of the computational cell. In a similar manner, difference expressions are obtained for the cross-flow momentum and energy equations. These relations are employed in the analysis whenever the local cross-flow velocity component becomes negative.

Shock-Wave/Boundary-Layer Interaction Analysis

The boundary-layer finite difference algorithm is employed to compute all of the forebody/centerbody and cowl boundary-layer flow except for that in the immediate vicinity of the shock-wave/boundary-layer interaction regions. An efficient three-dimensional integral analysis is used for determining the interaction region flow. The analysis solves integral forms of the continuity, streamwise momentum, and cross-flow momentum equations while assuming that the boundary-layer flow is isoenergetic immediately downstream of the shock-wave reflection. The analysis used in the present study represents an extension of the methods given in Refs. 20 and 21, and is applicable for weak interaction cases in which the flow does not separate.

The three-dimensional integral conservation equations are applied to a series of control volumes, where each control volume comprises a circumferential segment of the shock-wave/boundary-layer interaction region (see Fig. 4a). A given control volume is bounded by the current boundary-layer initial-value and solution surfaces in the streamwise ($\tilde{x}$) direction, and by the wall and the boundary-layer edge surfaces in the normal ($\tilde{y}$) direction.

Following the suggestion of Paynter,[21] the conservation equations are applied in a plane which is orthogonal to both the wall and to the space curve defined by the intersection of the shock wave with the wall. This plane is shown in Fig. 4b passing through the point P, and can be defined by the orthonormal triad of unit vectors $\hat{t}$, $\hat{n}_b$, and $\hat{\sigma}$. The vector $\hat{t}$ is tangent to the space curve at point P, $\hat{n}_b$ is orthogonal to the solid boundary at point P, and $\hat{\sigma}$ is orthogonal to both $\hat{t}$ and

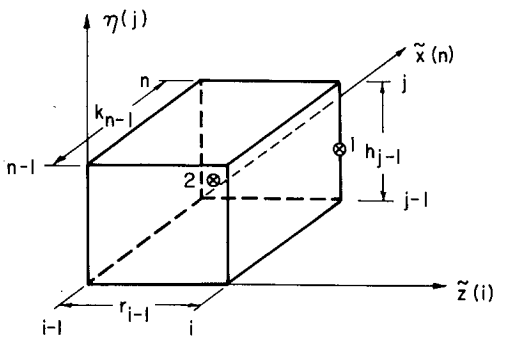

Fig. 2 Positive cross-flow computational network.

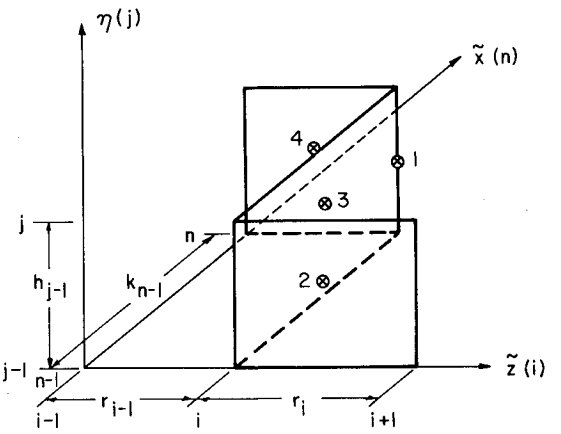

Fig. 3 Negative cross-flow computational network.

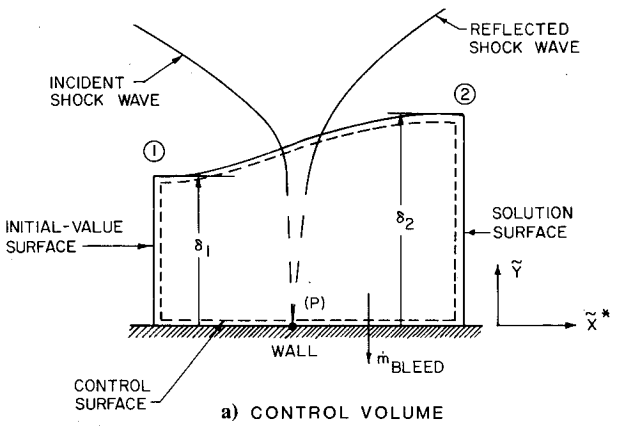

Fig. 4 Shock-wave/boundary-layer interaction region control volume and unit vectors.

$\hat{n}_b$ and is given by

$$\hat{o} = \hat{n}_b \times \hat{t} \tag{22}$$

The tangential unit vector $\hat{t}$ can be determined from

$$\hat{t} = (dx/ds)\,\hat{i} + (dy/ds)\,\hat{j} + (dz/ds)\,\hat{k} \tag{23}$$

where ds is the differential arc length along the space curve.

After the vector $\hat{o}$ has been determined, a coordinate rotation through the angle α is performed to obtain the upstream velocity components in the plane containing $\hat{n}_b$ and $\hat{o}$. The coordinate axes in and normal to this plane are denoted by $\tilde{x}^*$ and $\tilde{z}^*$, respectively, with the velocity components in these directions being denoted by $\tilde{u}^*$ and $\tilde{w}^*$, respectively.

The integral conservation equations are then applied to determine the boundary-layer property profiles on the downstream side of the interaction region. A cross section of the control surface used in the integral analysis is depicted in Fig. 4a, where the initial-value surface corresponds to station 1 and the solution surface corresponds to station 2. The integral conservation equations take the form

Continuity

$$\int_0^{\delta_1} \rho\tilde{u}^*\,d\tilde{y} = \int_0^{\delta_2} \rho\tilde{u}^*\,d\tilde{y} + \dot{m}_{\text{bleed}} \tag{24}$$

Streamwise momentum

$$P_1\delta_1 - P_2\delta_2 + \bar{P}(\delta_2 - \delta_1) = \int_0^{\delta_2} \rho(\tilde{u}^*)^2\,d\tilde{y} - \int_0^{\delta_1} \rho(\tilde{u}^*)^2\,d\tilde{y} \tag{25}$$

Cross-flow momentum

$$\int_0^{\delta_1} \rho\tilde{u}^*\tilde{w}^*\,d\tilde{y} = \int_0^{\delta_2} \rho\tilde{u}^*\tilde{w}^*\,d\tilde{y} \tag{26}$$

Energy

$$\bar{H}_1 = H_2 \tag{27}$$

In the preceding equations, the static pressure at stations 1 and 2 is assumed to be constant in the $\tilde{y}$ direction, and $\bar{P}$ is an appropriately weighted-average pressure acting on the upper surface of the control volume. It is assumed that negligible mass is entrained into the boundary layer between stations 1 and 2, that viscous shear stress effects may be neglected, and that mass bleed occurs normal to the wall.

Since the upstream flow properties have been determined by the finite difference algorithm, the integrals appearing in Eqs. (24-26) at station 1 are determined directly by numerical quadrature. To evaluate the integrals at station 2 requires that representations for the downstream velocity profiles be chosen. The following turbulent power law profiles were selected:

$$\tilde{u}^* = \tilde{u}_e^* \eta^{\beta_1} \tag{28}$$

$$\tilde{w}^* = \tilde{w}_e^* \eta^{\beta_2} \tag{29}$$

where

$$\eta = \tilde{y}/\delta \tag{30}$$

and the exponents β_1 and β_2 are in the range of 0 to 1.

The mean total enthalpy H may be expressed in terms of the mean static enthalpy h as

$$H = h + [(\tilde{u}_e^*)^2\eta^{2\beta_1} + (\tilde{w}_e^*)^2\eta^{2\beta_2}]/2 \tag{31}$$

Since both β_1 and β_2 are bounded and $(\tilde{w}_e^*)^2 \ll (\tilde{u}_e^*)^2$, Eq. (31) may be approximated as

$$h \cong H - \tfrac{1}{2}(\tilde{u}_e^*)^2\eta^{2\beta_1} \tag{32}$$

For a thermally and calorically perfect gas

$$\rho = \gamma P/(\gamma - 1)h \tag{33}$$

Equations (31-33) are substituted into Eqs. (24-27) to yield downstream integral expressions which are explicitly dependent on δ_2, β_1, and β_2.

To obtain the downstream property profiles, initial estimates are made for the exponents β_1 and β_2. Then Eqs. (24), (25), and (27) are combined to produce a system of two equations for δ_2 and β_1. These equations are solved using a Newton-Raphson iteration scheme with β_1 serving as the perturbation quantity. After convergence has been obtained for δ_2 and β_1, Eq. (26) is solved using a Newton-Raphson iteration scheme employing β_2 as the perturbation quantity. Determining δ_2, β_1, and β_2 defines the downstream property field. After the downstream velocity components $\tilde{u}_2^*$ and $\tilde{w}_2^*$ have been calculated, the velocity components $\tilde{u}_2$ and $\tilde{w}_2$ can be determined by a coordinate rotation.

By applying the analysis just given to a series of control volumes, the flow properties downstream of the shock-wave/boundary-layer interaction region may be determined for the entire computed sector. This solution is used as initial data for restarting the finite difference boundary-layer computation.

Overall Numerical Algorithm

Supersonic-Core Flow

An inverse marching scheme is employed in the supersonic flow algorithm. The solution is obtained on a family of space-like planes of constant x. The solution points on each plane represent the intersection points of continuous streamlines which are propagated from the data points specified on the initial-value plane. In addition to the streamline points, solution points are also obtained at the intersection of the external and internal shock waves with the solution plane, and for the internal flow on the space curves where the internal shock wave intersects the solid boundaries.

Boundary-Layer Flow

The overall algorithm for the boundary-layer computation consists of the repetitive application of the attachment line flow, three-dimensional flow, and shock-wave/boundary-layer interaction flow subalgorithms. The implicit finite difference algorithm is applied to compute all of the boundary-layer flow except for that in the shock-wave/boundary-layer interaction regions where the integral analysis is employed. The finite difference algorithm first applies the attachment line subalgorithm to calculate the boundary layer on the windward and leeward planes of symmetry. The three-dimensional flow subalgorithm is then applied to compute the boundary-layer flow between the planes of flow symmetry starting at the windward meridian and marching to the leeward meridian for a given solution surface.

Initial Data and Boundary Conditions

The supersonic flow initial data are specified on a plane of constant x. Many supersonic mixed-compression inlets

employ a centerbody whose initial contour is conical. The initial data for the flow about a circular cone at incidence may be obtained by employing the results of Jones.[22]

The boundary-layer flow initial data are specified at stations of constant $\bar{x}$. Separate sets of initial data must be specified to initiate the forebody/centerbody and cowl boundary-layer computations. If the forebody contour is conical ahead of the location where the computation is to be started, then the initial data may be generated using the implicit finite difference algorithm developed by Adams.[23] The cowl boundary-layer initial data must be specified at the axial location of the first supersonic flow solution plane inside the annulus (the boundary-layer thickness at the cowl lip is zero). The cowl boundary-layer initial data may be internally generated in the computer program using an approximate technique.

The computer program considers only axisymmetric contours. The body radius may be described either by tabular input or by using cubic splines. More arbitrary geometries can be incorporated by replacement of the existing geometry module.

The boundary-layer computation requires specification of the temperature or the normal-temperature derivative at the wall. Constant temperature or temperature derivative boundary conditions may be specified, or an arbitrary distribution may be specified by tabular input. Mass transfer boundary conditions are specified by entering the axial locations of the boundary-layer bleed zones and the mass flux within each zone.

Integration Step-Size Regulation

Except in the vicinity of an intersection of the internal shock wave with a solid boundary, the marching step between successive solution planes in the supersonic flow solution is determined by the Courant-Friedrichs-Lewy (CFL) stability criterion. In the vicinity of an intersection of the internal shock with a solid boundary, the axial step is chosen such that the shock-wave/solid-body intersection is contained between two adjacent solution planes.

The streamwise step size used in the boundary-layer computation is selected to correspond to the axial marching step. As a consequence, the supersonic flow and boundary-layer flow solutions are determined at the same axial stations. This appears to provide sufficient mesh resolution for calculating the boundary-layer development since, as the Mach number decreases and the static pressure increases, the marching step is automatically reduced.

Numerical Stability

A stability analysis of the nonlinear finite difference scheme for steady supersonic three-dimensional flow accounting for discrete shock fitting and molecular transport was not attempted. Instead, a stability analysis of the bicharacteristic scheme for steady three-dimensional isentropic flow was conducted. Stability of the generalized analysis was then verified by actual numerical calculations. Stability of the boundary-layer implicit finite difference algorithm was verified by actual numerical calculations.

Numerical Results

Internal flow results are now presented to illustrate application of the analysis. Numerical solutions are correlated with experimental data for the Boeing Mach 3.5 inlet[24,25] and the NASA P-inlet.[26,27] Both inlets are axisymmetric mixed-compression designs, and both employ translating centerbodies to alter the annulus goemetric throat area in accordance with flight conditions. For off-design operation, the centerbody must be translated forward of its design-point position either as the angle of attack α is increased or as the freestream Mach number M_∞ is reduced. This maintains supersonic flow through the throat and, thus, the inlet remains started. Both inlets have a design Mach number tolerance of 0.05. In the following discussion, the nondimensional centerbody translation required for off-design operation is denoted by $\Delta x/R_c$, where R_c is the cowl lip radius.

Both inlets employ boundary-layer bleed systems in the transonic throat region and upstream of the throat in the supersonic diffuser. This prevents separation and provides boundary-layer control in regions of strong adverse pressure gradients such as in the vicinity of oblique shock-wave/boundary-layer interactions. Distributed bleed systems are employed on both the centerbody and cowl.

Correlations for the Boeing Mach 3.5 Inlet

Comparisons of the computed internal surface pressure distributions and experimental data for the Boeing Mach 3.5 inlet operating at both design and off-design conditions are presented in Refs. 1 and 11. Comparisons of the computed boundary-layer development and experimental data for this inlet at zero angle of attack ($\alpha = 0$ deg) are presented in Figs. 5 and 6. The results presented in Fig. 5 correspond to an off-design freestream Mach number M_∞ of 2.1 at the centerbody translation of $\Delta x/R_c = 1.030$ and $M_\infty = 2.3$ at $\Delta x/R_c = 0.905$. Plotted is the stagnation pressure ratio P_T/P_{T_∞} (local stagnation/freestream stagnation) vs the nondimensional distance measured normal to the wall $\tilde{y}/L_R$ (distance/reference length). Results are presented for both the centerbody and cowl boundary layers at the axial stations denoted by x/R_c. Excellent agreement is obtained between analysis and experiment. The experimental data for the supersonic portion of each boundary layer have been corrected to account for the reduction in stagnation pressure across the normal shock wave induced by the boundary-layer rake probes. The correction was determined by interpolating the computed solution for the local Mach number at the location of a given rake probe and then using normal shock theory to compute the stagnation pressure loss across the shock wave. This stagnation pressure loss was then added to the originally measured stagnation pressure to give the corrected local stagnation pressure. No corrections are needed for probes in the subsonic portion of the boundary layer.

The experimental testing effort was conducted at freestream Mach numbers ranging from 0.6 to 3.5. The corresponding Reynolds numbers based on cowl lip diameter ranged from 2.8×10^6 at $M_\infty = 3.5$ to approximately 7×10^6 at the subsonic and transonic Mach numbers.[24] Following the discussion in Ref. 24, turbulent transition onset was assumed to occur at locations on both the centerbody and cowl where the local Reynolds number based on laminar momentum thickness equaled approximately 800. Assuming transition onset at positions upstream of these locations generally would result in overpredicting the respective displacement thicknesses. As noted earlier, a streamwise intermittency factor[15] was applied to better predict the progressive transition from laminar to turbulent flow.

Boundary-layer bleed was applied upstream of the cowl rake and was modeled in the analysis by specifying the bleed mass-flow rate (0.3% of the cowl lip mass-flow rate) and the axial extent of the bleed zone. The cowl boundary-layer rake was located downstream of the first shock-wave/boundary-layer interaction on the cowl. The centerbody rake was located upstream of the first shock-wave/boundary-layer interaction on the centerbody.

Figure 6 presents the computed boundary-layer stagnation pressure profiles and experimental data for the Boeing Mach 3.5 inlet at $M_\infty = 2.5$ and $\Delta x/R_c = 0.785$ and at $M_\infty = 2.7$ and $\Delta x/R_c = 0.611$. For the $M_\infty = 2.5$ case, the computed centerbody and cowl boundary-layer displacement thicknesses at the axial stations of the centerbody and cowl rakes were 0.17 cm and 0.046 cm, respectively. The corresponding measured values[24] were approximately 0.15 cm and 0.05 cm, respectively.

Wall static pressure measurements for the Mach 3.5 inlet

were made for both zero and nonzero incidence.[24,25] However, boundary-layer measurements were performed only for the zero incidence cases. Hence, the boundary-layer analysis/experiment correlations are limited to the zero incidence cases for this inlet.

Correlations for the NASA P-Inlet

The NASA P-inlet[26,27] has a design freestream Mach number of 2.65. Figure 7 compares the computed internal surface pressure distributions and experimental data for three off-design operating points for this inlet. Plotted is the pressure ratio P/P_{T_∞} (static/freestream stagnation) vs the nondimensional axial position x/R_c (axial position/cowl lip radius). The first off-design operating point has a freestream Mach number M_∞ of 2.38, zero angle of attack ($\alpha = 0$ deg), and a nondimensional centerbody translation $\Delta x/R_c$ of 0.516. The second off-design operating point has $M_\infty = 2.58$, $\alpha = 1.5$ deg, and $\Delta x/R_c = 0.218$. The third off-design operating point has $M_\infty = 2.58$, $\alpha = 3.0$ deg, and $\Delta x/R_c = 0.309$. In each case, results are presented for both the centerbody and the cowl. Good agreement is obtained between the results of the analysis and the experimental data.

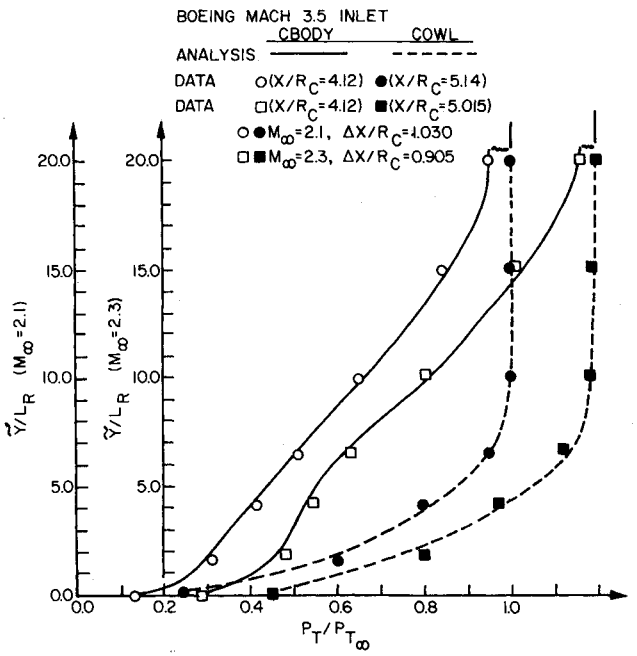

Fig. 5 Boeing Mach 3.5 inlet boundary-layer stagnation pressure profiles for $\alpha = 0$ deg and $M_\infty = 2.1$ and 2.3.

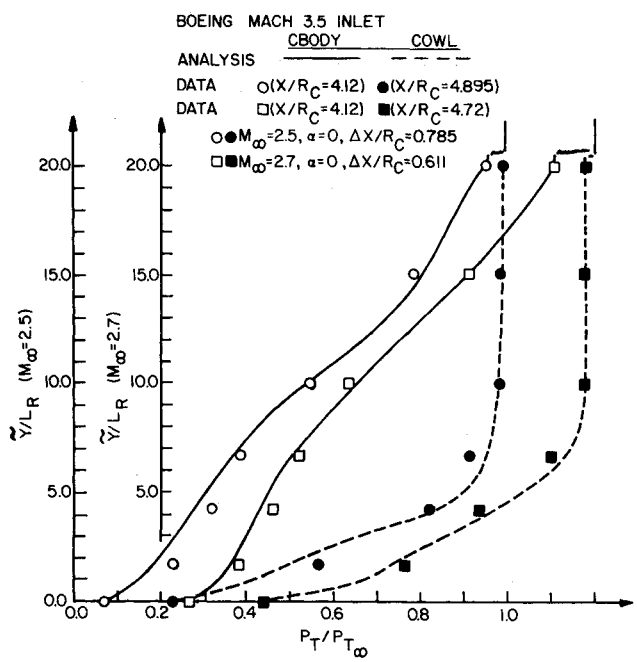

Fig. 6 Boeing Mach 3.5 inlet boundary-layer stagnation pressure profiles for $\alpha = 0$ deg and $M_\infty = 2.5$ and 2.7.

The results presented in Fig. 7 were obtained using the supersonic core flow bicharacteristic algorithm without viscous correction. The bicharacteristic algorithm is structured to allow specification of mass transfer boundary conditions at the wall. This option permits the effects of boundary-layer viscous entrainment to be approximated in the inviscid core flow algorithm by applying a surface transpiration velocity boundary condition which is determined from the computed boundary-layer growth. This technique has been successfully used in the prediction of transonic nacelle/inlet flowfields by Vadyak and Atta.[28] However, in view of the analysis/experiment correlations shown in Fig. 7, the viscous correction calculation did not seem to be warranted.

Correlations of the computed boundary-layer development and experimental data for the NASA P-inlet are presented in Fig. 8. Shown in this figure are the centerbody boundary-layer stagnation pressure profiles at the axial station $x/R_c = 3.68$ for three off-design cases, each case at zero incidence. The first case corresponds to $M_\infty = 2.18$, $\alpha = 0$ deg, and $\Delta x/R_c = 0.831$. The second case corresponds to $M_\infty = 2.28$, $\alpha = 0$ deg, and $\Delta x/R_c = 0.681$. The third case corresponds to $M_\infty = 2.38$, $\alpha = 0$ deg, and $\Delta x/R_c = 0.516$. In each case, good agreement is obtained between analysis and experiment.

The experimental tests for the P-inlet were conducted at freestream Mach numbers ranging from 2.0 to 2.6. Tunnel conditions were altered to provide a constant characteristic Reynolds number of 8.2×10^6/m (2.5×10^6/ft) across the test Mach number range.[26] Turbulent transition onset was taken as occurring at the axial location where the Reynolds number based on laminar momentum thickness was in the range of 500-700. No bleed was employed upstream of the centerbody boundary-layer rake.

Figure 9 compares the computed boundary-layer stagnation pressure profiles and experimental data for the leeward meridian for two off-design cases at incidence. The first case corresponds to $M_\infty = 2.18$, $\alpha = 1.5$ deg, and $\Delta x/R_c = 0.850$.

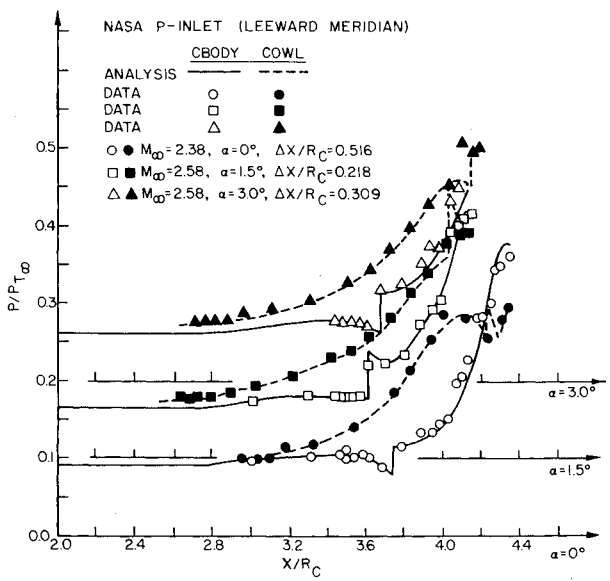

Fig. 7 NASA P-inlet internal surface pressure distributions.

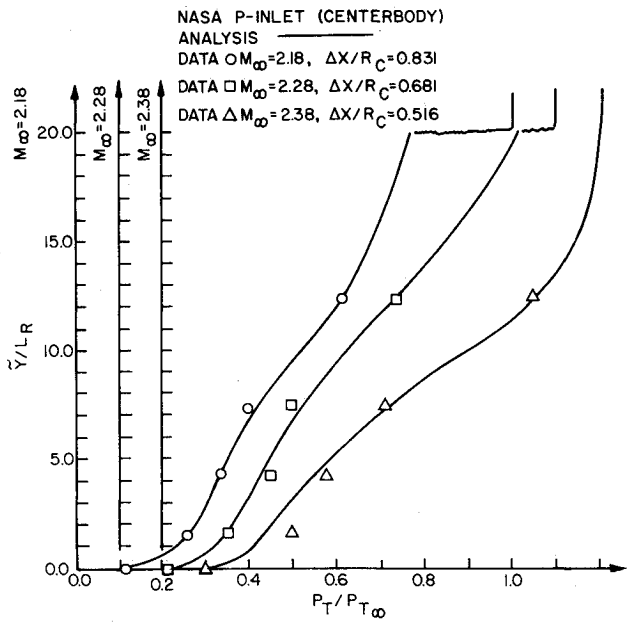

Fig. 8 NASA P-inlet boundary-layer stagnation pressure profiles for $x/R_c = 3.68$, $\alpha = 0$ deg, and $M_\infty = 2.18$, 2.28, and 2.38.

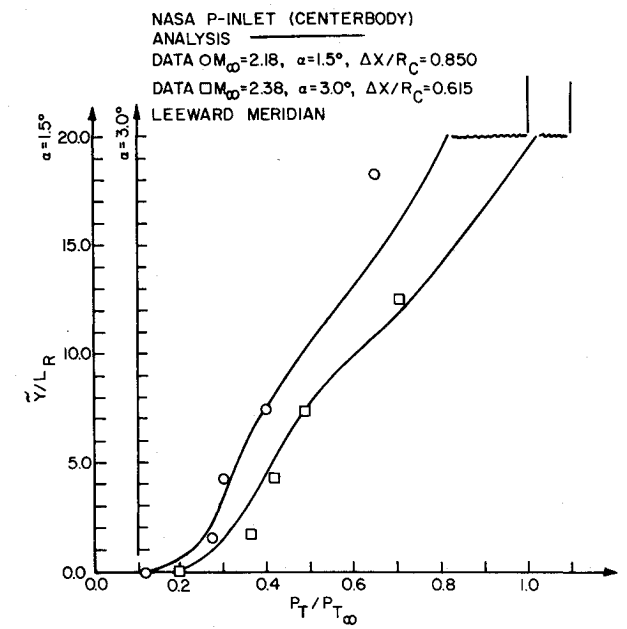

Fig. 9 NASA P-inlet boundary-layer stagnation pressure profiles for $x/R_c = 3.68$ and $\alpha = 1.5$ and 3.0 deg.

The second case corresponds to $M_\infty = 2.38$, $\alpha = 3.0$ deg, and $\Delta x/R_c = 0.615$. Good agreement is obtained between the numerical results and experiment.

Computer Execution Time and Computational Grid

Three-dimensional flow solutions, including both the supersonic core flow computation and centerbody and cowl boundary-layer computations, typically require about 50 min of CPU execution time on the VAX-11/780 computer if the solution is initiated at the cowl lip axial station. Typically, 15 circumferential stations and 11 radial stations are used in the supersonic core flow solution, and 15 circumferential stations and 20 normal stations are used in the boundary-layer computation. Options exist in the program to defeat the boundary-layer computation, or to compute just the external or internal flowfields. The algorithm is executed for three-dimensional flows assuming one plane of flow symmetry. An option exists which permits the rapid computation of axisymmetric flows.

Conclusions

An analysis has been presented for calculating the three-dimensional flowfield in supersonic mixed-compression inlets operating at angle of attack. The solution is obtained using a zonal modeling approach which employs separate analyses for each of the different computational regimes. The culmination of this research endeavor is the development of a production-type computer program which is available and which has the capability to predict the flowfield in a variety of mixed-compression inlets. The results produced by the present analysis agree well with experimental data for both axisymmetric and three-dimensional flowfields.

Acknowledgments

This research effort was sponsored by the NASA Lewis Research Center under Grant NSG-3311. The authors wish to express their appreciation to Mr. Jan Syberg of the Boeing Company and Mr. Joseph Wasserbauer of NASA Lewis for supplying the experimental data used in performing the correlations.

References

[1] Vadyak, J. and Hoffman, J. D., "Calculation of the Flow Field Including Boundary Layer Effects for Supersonic Mixed-Compression Inlets at Angle of Attack," NASA CR-167941, 1982. (see also: Vadyak, J. and Hoffman, J. D., "A Computer Program for the Calculation of the Flow Field Including Boundary Layer Effects for Supersonic Mixed-Compression Inlets at Angle of Attack," NASA CR-168002, 1982).

[2] Sorensen, V. L., "Computer Program for Calculating Flow Fields in Supersonic Inlets," NASA TN D-2897, 1965.

[3] Anderson, B. H., Tassa, Y., and Reshotko, E., "Characteristic Procedure for Supersonic Flows Including Consideration of Viscous Contributions to Flow Rotationality," AIAA Paper 76-426, 1976.

[4] Reyhner, T. A. and Hickcox, T. E., "Combined Viscous-Inviscid Analysis of Supersonic Inlet Flowfields," *Journal of Aircraft*, Vol. 9, Aug. 1972, pp. 589-595.

[5] Knight, D. D., "Calculation of High-Speed Inlet Flows Using the Navier-Stokes Equations," *Journal of Aircraft*, Vol. 18, Sept. 1981, pp. 748-754.

[6] MacCormack, R. W., "The Effect of Viscosity in Hypervelocity Impact Cratering," AIAA Paper 69-354, 1969.

[7] Presley, L. L., "Internal Flow Calculations for Axisymmetric Supersonic Inlets at Angle of Attack," AIAA Paper 75-1214, 1975.

[8] Buggeln, R. C., McDonald, H., Kreskovsky, J. P., and Levy, R., "Computation of Three-Dimensional Viscous Supersonic Flow in Inlets," AIAA Paper 80-0194, 1980.

[9] Vadyak, J. and Hoffman, J. D., "Calculation of the Flow Field in Supersonic Mixed-Compression Inlets at Angle of Attack Using the Three-Dimensional Method of Characteristics with Discrete Shock Wave-Fitting," NASA CR-135425, 1978.

[10] "Advanced Concept Studies for Supersonic Vehicles," The Boeing Company, NASA CR-159244, 1980.

[11] Vadyak, J., Hoffman, J. D., and Bishop, A. R., "Flow Computations in Inlets at Incidence Using a Shock Fitting Bicharacteristic Method," *AIAA Journal*, Vol. 18, Dec. 1980, pp. 1495-1502.

[12] Butler, D. S., "The Numerical Solution of Hyperbolic Systems of Partial Differential Equations in Three Independent Variables," *Proceedings of Royal Society of London*, Vol. A255, 1960, pp. 232-252.

[13] Vaglio-Laurin, R., "Turbulent Heat-Transfer on Blunt-Nosed Bodies in Two-Dimensional and General Three-Dimensional Hypersonic Flow," *Journal of the Aerospace Sciences*, Vol. 27, Jan. 1960, pp. 27-36.

[14] Cebeci, T., Kaups, K., Mosinskis, G. J., and Rehn, J. A., "Some Problems of the Calculation of Three-Dimensional Boundary Layer Flows on General Configurations," NASA CR-2285, 1973.

[15] Dhawan, S. and Narasimha, R., "Some Properties of Boundary Layer Flow During the Transition from Laminar to Turbulent Motion," *Journal of Fluid Mechanics*, Vol. 3, April 1958, pp. 418-436.

[16]Moore, F. K., *Theory of Laminar Flows,* Vol. IV, Princeton University Press, Princeton, N.J., 1964.
[17]Keller, H. B., "A New Difference Scheme for Parabolic Problems," *Numerical Solution of Partial Differential Equations,* Vol. II, Academic Press, New York, 1970.
[18]Cebeci, T., Khattab, A. A., and Stewartson, K., "Studies on Three-Dimensional Boundary Layers on Bodies of Revolution; Three-Dimensional Laminar Boundary Layers and the Ok of Accessibility," Rept. MDC J8716, Douglas Aircraft Co., Long Beach, Calif., 1980.
[19]Raetz, G. S., "A Method of Calculating Three-Dimensional Laminar Boundary Layers of Steady Compressible Flow," Rept. NAI 58-73, Northrop Corp., Los Angeles, Calif., 1957.
[20]Syberg, J. and Koncsek, J. L., "Bleed System Design Technology for Supersonic Inlets," *Journal of Aircraft,* Vol. 10, July 1973, pp. 407-413.
[21]Paynter, G. C., "Analysis of Weak Glancing Shock/Boundary Layer Interactions," AIAA Paper 79-0144, 1979.
[22]Jones, D. J., "Numerical Solutions of the Flow Field for Conical Bodies in a Supersonic Stream," Rept. LR-507, National Research Council of Canada, 1968.
[23]Adams, J. C., "Finite Difference Analysis of the Three-Dimensional Turbulent Boundary Layer on a Sharp Cone at Angle of Attack in a Supersonic Flow," AIAA Paper 72-186, 1972.
[24]Syberg, J. and Koncsek, J. L., "Experimental Evaluation of a Mach 3.5 Axisymmetric Inlet," NASA CR-2563, 1975.
[25]Koncsek, J. L., "Machine Plot Supplement to D6-42494," Rept. D6-42595, The Boeing Company, Seattle, Wash., 1975.
[26]Syberg, J. and Turner, L., "Supersonic Test of a Mixed-Compression Axisymmetric Inlet at Angles of Incidence," NASA CR-165686, 1981.
[27]Results from the Testing Program for the NASA P-Inlet Conducted at NASA Lewis Research Center, private communication with Joseph Wasserbauer, 1982.
[28]Vadyak, J. and Atta, E. H., "Three-Dimensional Transonic Nacelle/Inlet Flowfield Computations Using an Efficient Approximate Factorization Algorithm," AIAA Paper 83-1417, 1983.